NANO LETTERS

Letter

pubs.acs.org/NanoLett

Giant Coupling Effect between Metal Nanoparticle Chain and Optical Waveguide

Mickaël Février,[†,⊥] Philippe Gogol,[†,⊥] Abdelhanin Aassime,[†,⊥] Robert Mégy,[†,⊥] Cécile Delacour,[‡,∥] Alexei Chelnokov,[‡] Aniello Apuzzo,[§] Sylvain Blaize,[§] Jean-Michel Lourtioz,[†,⊥] and Béatrice Dagens*[,†,⊥]

[†]Univ Paris-Sud, Institut d'Electronique Fondamentale, UMR 8622, 91405 Orsay cedex, France

[⊥]CNRS, 91405 Orsay cedex, France

[‡]CEA-LETI, MINATEC, DOPT, 17 rue des Martyrs 38054 Grenoble cedex 9, France

[§]Laboratoire de Nanotechnologie et d'Instrumentation Optique, Institut Charles Delaunay, CNRS-UMR 6279, Université de Technologie de Troyes, BP 2060, 10010 Troyes, France

S *Supporting Information*

ABSTRACT: We demonstrate that the optical energy carried by a TE dielectric waveguide mode can be totally transferred into a transverse plasmon mode of a coupled metal nanoparticle chain. Experiments are performed at 1.5 μm. Mode coupling occurs through the evanescent field of the dielectric waveguide mode. Giant coupling effects are evidenced from record coupling lengths as short as ~560 nm. This result opens the way to nanometer scale devices based on localized plasmons in photonic integrated circuits.

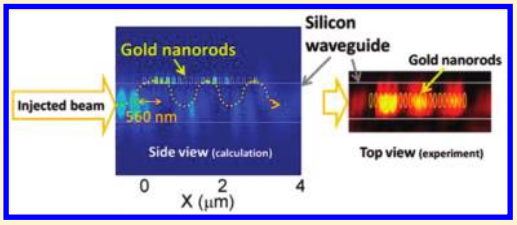

KEYWORDS: *Surface plasmon polariton, localized surface plasmon, silicon photonics, plasmonics, integrated optics*

Energy transfer via dipolar interactions between closely spaced metal nanoparticles (MNPs) leads to the formation of a highly confined waveguide operated below the diffraction limit.[1,2] Until now, light propagation along coupled MNP chain has been achieved using Kretshman−Raether,[3] near-field,[4] or plane wave[5−7] excitation, exploring in most cases the MNP chain waveguide dispersion curves inside the light cone. Yet, the excitation of localized surface plasmons (LSP) in guided configuration remains a crucial step toward a true implementation of plasmonic functions in photonic integrated circuits (PICs). One important challenge for today's photonics is indeed the realization of highly miniaturized integrated circuits capable of very large scale integration of optical functions, combined with electronics.[8] While silicon waveguides allow for a strong confinement of light and an almost transparent propagation, lossy surface plasmon waveguides can ultimately exhibit small dimensions at the nanometer scale.[9−11] Combining both waveguides then appears to be of great promise. Within plasmonic world, localized surface plasmons potentially offer a wide variety of configurations since metallic nanoparticles can be arranged on demand on a substrate[2,12] or a waveguide. Resonant dipole excitation and field confinement in MNPs open the way to enhance optical (nonlinear) interactions.[13−16] In all cases, short MNP chains should be used, but an efficient LSP excitation is then needed.

In this work, LSP excitation is achieved by using strong coupling effects between a Si waveguide and a chain of gold nanoparticles that are deposited on top (Figure1a). Excitation occurs through the evanescent field of the fundamental TE waveguide mode. A transverse plasmonic mode T_1 is then excited along the MNP chain.[6] We demonstrate that giant coupling between MNPs and the silicon waveguide can be obtained in this configuration as illustrated by a periodic transfer of light from one guide to the other with record characteristic lengths as short as ~560 nm. This behavior is shown to occur only if a collective (or long distance) oscillation of the dipoles is achieved along the chain, in other words, if a specific mode of the entire chain is excited.[5,6]

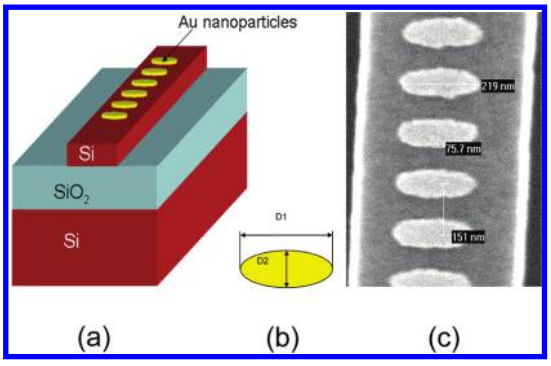

Figure 1. Experimental sample: (a) schematic view of a gold nanoparticle chain on top of a SOI waveguide; (b) picture showing the ellipsoidal shape of nanoparticles with *D*1 (respectively *D*2) the long (respectively small) axis size; (c) scanning electron micrograph of 6 gold nanorods of a 20-nanoparticle chain.

Received: December 4, 2011
Revised: January 9, 2012
Published: January 17, 2012

Silicon ridge waveguides with 220 × 500 nm^2 cross section were used in our experiments. The waveguides are single-mode above λ = 1.4 μm. Gold nanoparticle chains were fabricated using electron-beam lithography followed by a lift-off process. A 1 nm thick titanium (Ti) adhesion layer and a 30 nm gold layer were deposited by electron-beam evaporation. Figure 1b,c shows 6 MNPs of a 20 ellipsoïdal particles chain with axis dimensions D_1 = 220 ± 5 nm and D_2 = 75 ± 5 nm. As seen, the MNPs are precisely aligned along the symmetry axis of the Si waveguide. Center-to-center distance between particles is equal to 150 nm. The 3 μm long MNP chain is located at equal distance between the two waveguide facets.

The mentioned size and spacing of nanoparticles were previously determined by using 3D finite-difference time-domain (FDTD) simulations. The model incorporates measured parameters of the fabricated structures. Accurate dispersion data were used for the deposited gold layers after fitting a Drude model to ellipsometric measurements. The presence of a thin layer of native oxide between Si and Ti was also accounted for in FDTD calculations. For our technological process, the layer thickness was measured to be 3 nm by scanning electron microscopy. All FDTD simulations in this work were using these input data and a 3D mesh with dimensions smaller than 2 nm in the MNP region. Nanoparticle size and spacing were chosen in such a way that the chain resonance occurs in the transmission window of the silicon waveguide (λ > 1.2 μm) with an excitation by the TE waveguide mode and a dipolar coupling between neighboring particles. The ellipsoidal nanorod shape for nanoparticles with the long axis perpendicular to propagation direction (Figure 1b) was identified as an appropriate shape, compatible with fabrication process. The center to center spacing of 150 nm allows optimized dipolar coupling.

The excitation of gold nanoparticle chains was analyzed in three ways. First of all, by measuring the transmission spectra of Si waveguides decorated with gold nanoparticles; then by experimentally determining the near-field maps for excited MNP chains; and finally by using FDTD simulations for the interpretation of measurements.

The transmission spectra of MNP chain/Si waveguide systems were measured by injecting a polarized light to the butt facet of the Si waveguide using a lensed fiber (Figure 2a). A reference waveguide without MNP was used for transmission normalization. The input light was delivered by a tunable laser scanned by steps of 1 nm over the 1260−1630 nm range. Figure 3a shows the normalized transmission spectrum of a 20-particles chain. A transmission minimum is observed at 1475 nm, which corresponds to the maximum excitation of nanoparticles leading to the highest ohmic losses. "Noise" on the experimental curve is due to Fabry−Perot oscillations caused by reflections at the waveguide ends (see Supporting Information). Numerical simulations were performed by using described FDTD model. As seen, there is a very good agreement between calculations and measurements. The slightly broader resonance found in measurements is readily explained by the size distribution of MNPs.

The FDTD model was further exploited to calculate the field intensity defined as $|E|^2$ along the MNP chain and the Si waveguide. Figure 3c,d,e (left) shows field intensity maps in the vertical symmetry plane of the structure for three wavelengths, 1375, 1475, and 1575 nm, respectively. A periodic energy transfer between the Si waveguide and the MNP chain is clearly seen at 1475 and 1575 nm with an exponential decrease due to

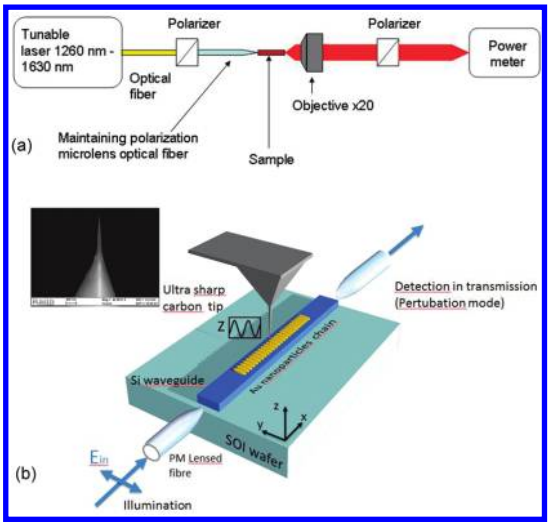

Figure 2. Experimental setup: (a) guided optic setup for transmission measurements; (b) TraNSOM setup used for the optical near-field measurement. See Supporting Information for more detailed description.

metal losses. The field intensity periodically falls near zero in the Si waveguide while it simultaneously reaches a maximum in the MNP chain. The transfer is almost total at 1475 nm. The transfer is only partial at 1575 nm. For both wavelengths, the MNP chain and the Si waveguide behave as two almost balanced coupled waveguides. A completely different behavior is found at 1375 nm since no oscillation is visible along the structure. Let us notice that a reflected signal exists for the three wavelengths due to the impedance mismatch between the bare Si waveguide and the waveguide section with MNPs. However, the signal amplitude remains below 10%.

Calculations of Figure 3c,d,e (left) were qualitatively verified from near field measurements. For this purpose, an aperturless transmission-based near-field scanning optical system equipped with an AFM was used (Figure 2b) to image the near field profile of optical modes propagating along the structure. Images corresponding to the three representative wavelengths 1375, 1475, and 1575 nm are shown in Figure 3c,d,e (right). In the three cases, the optical near-field images well reproduce the field intensity distribution calculated along the MNP chain. A periodic excitation of MNPs is clearly detected at 1475 and 1575 nm with the same period as in FDTD simulations. This good agreement between simulations and near-field images emphasizes the fact that the AFM probe perturbation remains negligible. In other words, the perturbation induced by the AFM probe does not significantly modify the modal behavior of the photonic structure. This small-perturbation condition is obtained by using an ultrasharp AFM tip (high density carbon nanotip from Nanotools) working in intermittent contact mode.[17]

The beating period is estimated to be 1.15 μm peak-to-peak. This oscillation is not correlated to Fabry−Perot like reflections at the Si waveguide ends since it is wavelength independent over the entire wavelength range from 1475 to 1575 nm. Moreover, in agreement with theoretical predictions, the periodic excitation of MNPs disappears at short wavelengths. Lateral (but not longitudinal) oscillations observed at 1375 nm (Figure 3c, right) can be attributed to a bimodal (TE00, TE01) behavior of the Si waveguide. These two-mode oscillations were not taken into account in simulations but explain decreasing

dx.doi.org/10.1021/nl204265f | Nano Lett. 2012, 12, 1032−1037

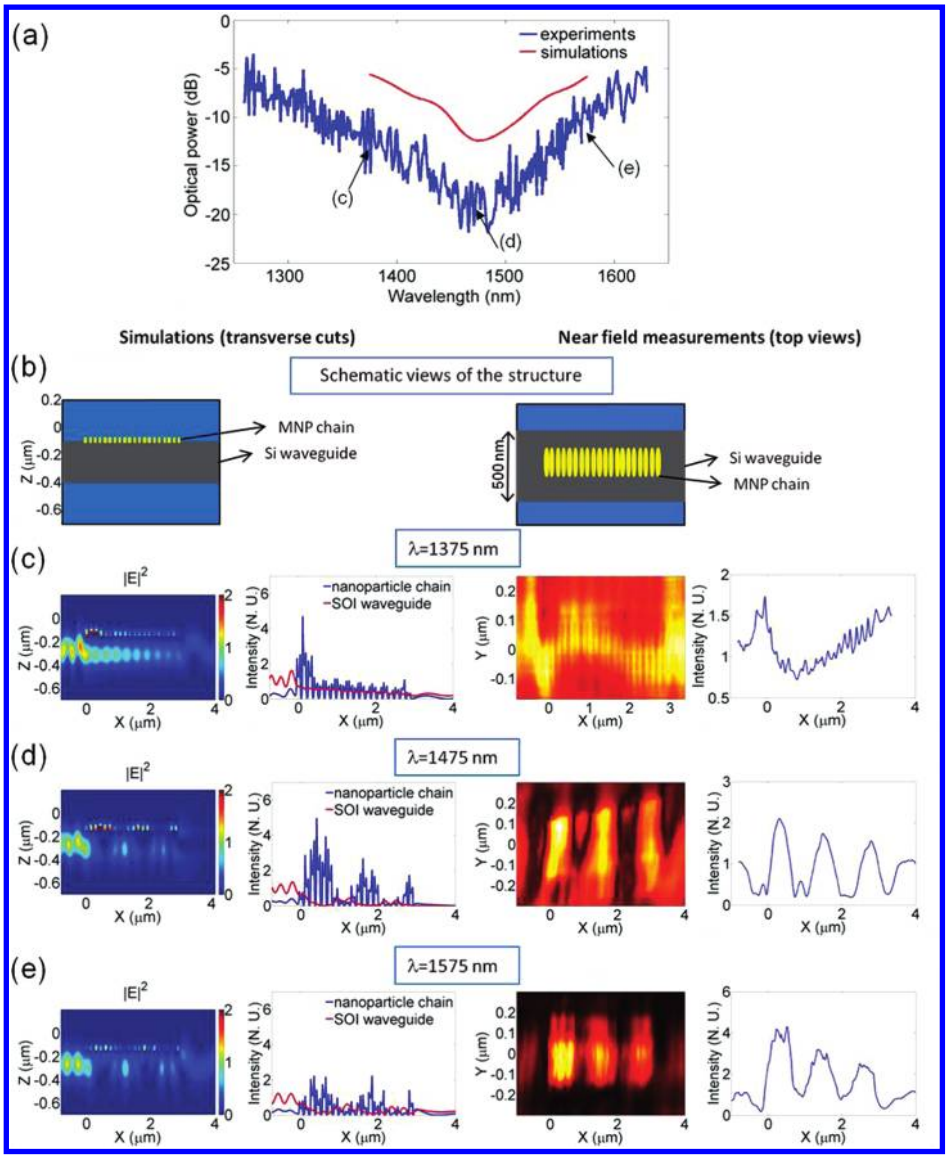

Figure 3. Experimental and theoretical results obtained with the 20 MNP chain on silicon waveguide. (a) Waveguide transmission measurements and FDTD simulations. (b–e) Field intensity calculations (left) and near-field measurements (right). Schematic views of the structure are recalled in (b). Panels c, d, and e are obtained at λ = 1375, 1475, and 1575 nm, respectively. The electric field intensity maps (leftmost column) are calculated in the vertical symmetry plane of the structure (at $y \sim 0$ μm). The corresponding intensity profiles are shown in the middle left column for both the nanoparticle chain (blue) and the Si waveguide (red). The measured near-field top views and the corresponding near-field intensity profiles (at $y \sim 0$ μm) are shown in the middle right and rightmost columns, respectively.

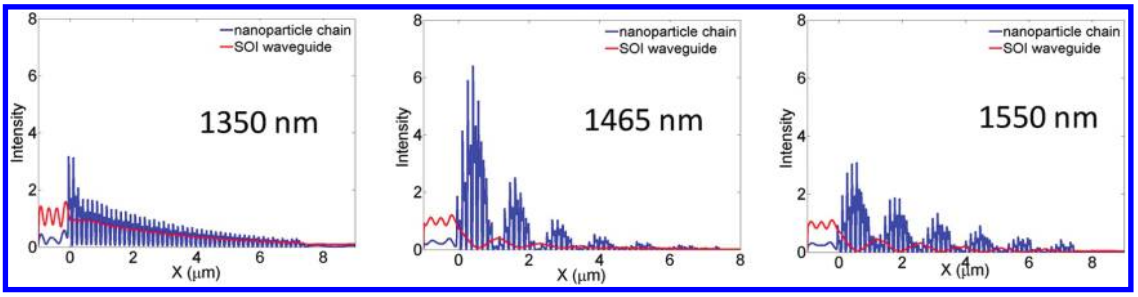

Figure 4. Field intensity calculations for a 50 MNP long chain at 1350, 1465, and 1550 nm.

and increasing intensity between x = 0 and 2 μm when measured at fixed $y \sim 0$ μm (Figure 3c, rightmost).

An additional evidence of mode coupling between the Si waveguide and the MNP chain is given in Figure 4, which shows FDTD calculations for a 50 MNP long chain. Here again, a periodic energy transfer between the Si waveguide and the MNP chain occurs at λ = 1465 and 1550 nm with the same period as in Figure 3d,e. Because of the longer chain, six periods are found instead of three. In contrast, a monotonous decrease of the field intensity is observed at λ = 1350 nm.

dx.doi.org/10.1021/nl204265f | *Nano Lett.* 2012, 12, 1032–1037

Coupled-mode theory provides an analytical framework to interpret the results of Figures 3c,d,e and 4. Although MNPs obviously induce high ohmic losses with an exponential decrease of the transmitted power along the chain, coupling effects can be analyzed in first approximation within the lossless coupled-mode theory while neglecting the imaginary parts of propagation constants. Because of the high proximity of the two waveguides and of the resonant behavior of the MNP chain, overlap integrals of the electromagnetic fields cannot be neglected in our case, and the coupling constants are not identical. Improved coupled-mode theory[18,19] establishes that in the case of strongly coupled waveguides a and b, ("a" corresponding to the waveguide where the input signal is injected) the normalized optical powers in a and b, P_a and P_b, evolve along the propagation axis x as follows:

$$P_a = 1 - \left(\frac{1 - C_{ab}C_{ba}}{1 + \delta^2}\right) e^{2\sinh^{-1}\left(\frac{C_{ab}+C_{ba}}{2}\delta\right)} \sin^2\left(\sqrt{\kappa_{ab}\kappa_{ba}(1 + \delta^2)}\, x\right) \quad (1)$$

$$P_b = C_{ab}C_{ba} + \left(\frac{1 - C_{ab}C_{ba}}{1 + \delta^2}\right) \sin^2\left(\sqrt{\kappa_{ab}\kappa_{ba}(1 + \delta^2)}\, x\right) \quad (2)$$

where κ_{ab}, κ_{ba} and δ are, respectively, the extended coupling constants and the asynchronism factor, which themselves include the contribution of the overlap integrals C_{ab} and C_{ba} (see Supporting Information). Using eqs (1) and (2), it appears that the energy transfer to waveguide b (the 20 MNP chain in our case) can be total only for $\delta = 0$. Such a transfer occurs at $x = \pi/(\kappa_{ab}\kappa_{ba})^{1/2}$. FDTD simulations show that the energy transfer is very close to 100% at 1475 nm and that the coupling length (i.e., half the oscillation period) is equal to ~560 nm. The average coupling constant $(\kappa_{ab}\kappa_{ba})^{1/2}$ at this wavelength thus reaches the giant value of ~2805 mm^{-1}, which is 1.5 times higher than that in the case of a coupling to a slot plasmonic waveguide.[20] A nonzero δ value at 1575 nm does not significantly change the coupling period since $(\kappa_{ab}\kappa_{ba})^{1/2}$ is the dominant term in eq 2. Extended coupled-mode theory also predicts that for non-negligible overlap integrals, the power maximum in waveguide b does not coincide with the power minimum in waveguide a. This is well verified from FDTD simulations in Figure 3d,e.

The absence of mode coupling between the Si waveguide and the MNP chain at 1375 nm can be interpreted in two ways. One interpretation is that phase matching conditions cannot be achieved between the two guides. Another explanation is that a collective excitation of dipoles along the chain cannot exist at this wavelength.

Field maps obtained from FDTD calculations have been analyzed in detail to identify the correct interpretation. In what follows, we will first examine the dispersion curves extracted from these calculations. The excitation of dipoles along the chain will be investigated in a second step from the complex field maps.

The spatial Fourier transform of the complex field was calculated in the midplane of the MNP chain for different frequencies. The dispersion curves of the excited modes were then retrieved from these calculations. Results are reported in Figure 5 with colors from blue to red corresponding to different amplitude levels of the wavevector components after Fourier transformation. The dispersion diagram actually represents the supermodes as defined in the coupled mode theory. The separation between the two branches in this diagram results from an anticrossing phenomenon due to the interaction between the stand-alone silicon waveguide TE mode and the MNP chain modes. The red dotted line in Figure 5 is the true dispersion curve of the stand-alone Si waveguide TE00 mode derived from standard calculations. The red dashed line simulates the dispersion curve of the MNP chain in the region where collective LSP modes are excited; by construction, it is tangent to the higher dispersion branch at low frequencies and follows the slight curvature of the lower dispersion branch at high frequencies. Clearly, we are led to the conclusion that anticrossing occurs well below the maximum frequency explored in our experiments. The slight curvature of the lower dispersion branch also suggests the existence of a maximum frequency in the MNP chain dispersion curve. Reported literature on MNP chain dispersion curves show that there is indeed a minimum wavelength (i.e., a maximum frequency) for the existence of a chain mode.[21−23]

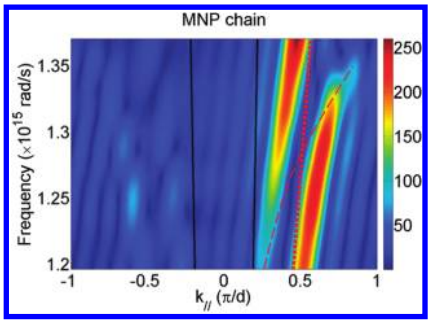

Figure 5. Dispersion curves of excited modes extracted from the spatial Fourier transform of the complex electric field calculated in the midplane of the MNP chain. Black lines delimit the light cone. Red dotted line is the silicon waveguide TE00 mode dispersion curve. Red dashed line is a guide for the eyes representing the dispersion curve of the MNP chain.

Let us now examine the very nature of plasmonic excitations. Figure 6a,b shows the field intensity profiles calculated in the midplane of the 20 MNP chain at 1375 and 1475 nm, respectively. As seen, the field intensity concentrates at the extremities of each excited MNP, thereby indicating the dipolar nature of the excitation. Figure 6c−f shows top-view maps of the y and z components of the electric field (real part) calculated in the midplane of the MNP chain. Electric-field characteristics and orientations are also typical of a dipolar excitation. The E_z component is oriented into opposite directions at the two extremities of each nanoparticle whereas the E_y component has the same orientation at these extremities. The electric field lines around each MNP then close up via the Si "substrate". The existence of collective excitations along the MNP chain can be discussed from a detailed inspection of the E_z component in Figure 6e,f. At short wavelengths (λ = 1375 nm, Figure 6e), the field maxima (respectively minima) observed along the MNP chain exactly coincide with the maxima (respectively minima) of the evanescent Si-waveguide-mode field numerically detected at the periphery of the particles (at $|y| > 0.2$ μm). Two interpretations are possible. Either the **k**-vectors of the Si and MNP waveguide modes are perfectly matched to each other and the propagating phases are then identical, or the MNP chain does not behave as a waveguide (i.e., there is no collective oscillation of dipoles) and

dx.doi.org/10.1021/nl204265f | Nano Lett. 2012, 12, 1032−1037

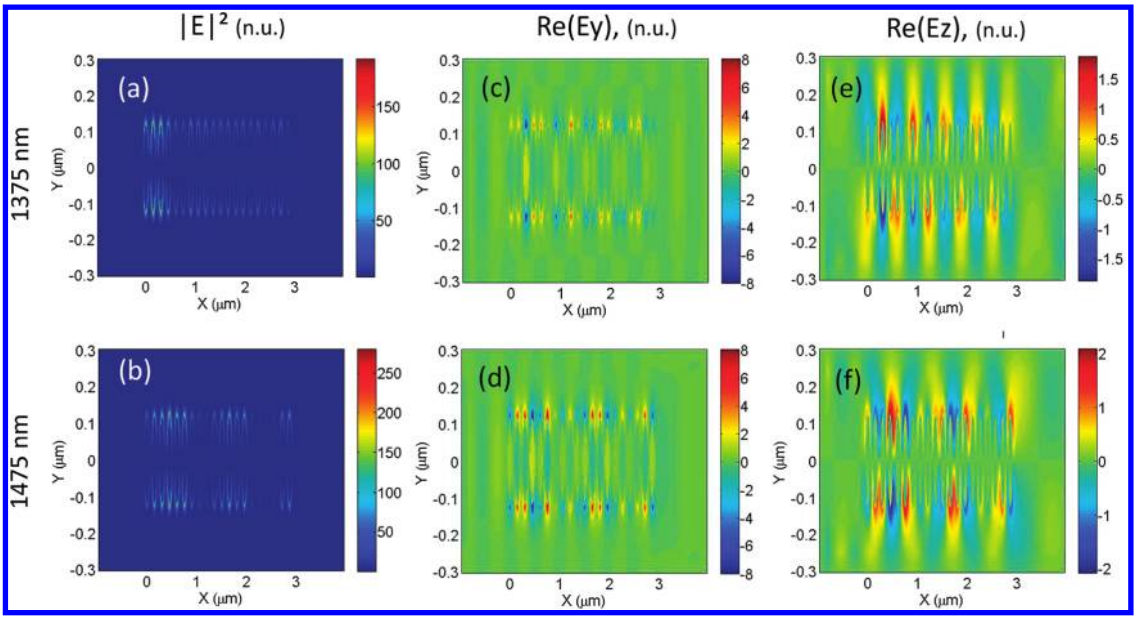

Figure 6. Top view of gold nanoparticle chain excitation (FDTD). (a,b) Field intensity profiles calculated in the midplane of the 20 MNP chain at 1375 and 1475 nm, respectively; (c–f) Top-view maps of the *y* and *z* components of the electric field (real part) in the midplane of the MNP chain.

each dipole is excited individually with the dipole orientation dictated by the electric field propagating in the Si waveguide. The first possibility is excluded since perfect phase matching should be accompanied by a periodic energy transfer from one guide to the other. Therefore we can conclude that the dipole excitation is simply the consequence of the near frequency coincidence between the Si waveguide mode and the LSP resonance of individual nanoparticles. The absence of collective MNP excitation at this wavelength is then confirmed. In consequence, results of Figure 3c cannot be explained by the absence of **k**-vector matching at 1375 nm.

The situation is different at 1475 nm and at longer wavelengths. The field maxima (respectively minima) at the MNP extremities (Figure 6f) do not exactly coincide with the maxima (respectively minima) observed for the evanescent Si-waveguide-mode field (at $|y| > 0.2$ μm). The wavevectors of the MNP chain and Si waveguide modes are then somewhat different. In other words, the MNP chain supports at least one proper waveguide mode, which can be identified as a collective LSP mode. This agrees with the interpretation of the results of Figure 3d,e and 4 in terms of strong coupling between two waveguide modes with one mode associated to a collective oscillation of MNP dipoles.

In conclusion, interfacing of a dielectric waveguide with a localized surface plasmon waveguide has been analyzed both experimentally and numerically in a configuration where a gold nanoparticle chain was excited via the evanescent field of a TE silicon waveguide mode. Three-dimensional FDTD simulations have been found to match very well to transmission and near-field measurements. We have shown that a collective oscillation of the metallic dipoles, characteristic of a true LSP chain mode, can occur only within a limited spectral range. A giant coupling is then achieved between the dielectric and plasmonic guides. This in turn allows for a highly efficient excitation of a metal nanoparticle chain over a very short distance. Here the coupling length is very close to the wavelength in the silicon waveguide. Since propagation losses decrease with the interaction distance, short MNP chains represent an attractive way to implement LSP based integrated optical devices with nanometer sizes and moderate losses in photonic circuits. In addition, the waveguide configuration allows using the entire optical energy available at the waveguide input for launching the plasmon in the coupled MNP chain. The use of long dielectric waveguides would also allow positioning optical sources and detectors far from the plasmonic section, thus providing an independent access to this section for optical sensing and biodetection. Moreover, thanks to the periodic "recoupling" of the propagating wave from the coupled MNP chain to the dielectric waveguide, optical loss in the plasmonic section(s) could be compensated for by implementing an amplifier medium in the dielectric waveguide. Finally, this work opens the way to ultracompact optical functions in guided photonics by locally using nonlinear and/or enhanced effects induced by dipolar excitation in MNPs. The energy carried by a guided mode can be almost totally transferred into a single MNP at the end of a short MNP chain. Magneto-optical effects,[24] wavelength conversion,[13] particle tweezing,[16] and biodetection[25] could also be envisaged by exploiting short metal nanoparticle chains in waveguide configuration.

■ ASSOCIATED CONTENT

Ⓢ Supporting Information

Supporting Information include the following topics: (1) transmission measurements description, (2) optical near-field mapping details, and (3) extended coupled-mode theory. This material is available free of charge via the Internet at http://pubs.acs.org.

■ AUTHOR INFORMATION

Corresponding Author

*E-mail: beatrice.dagens@ief.u-psud.fr. Phone: +33(0) 169157837. Fax: +33(0)169154000.

Present Address

[‖]Institut Neel, CNRS, 25 rue des Martyrs 38042 Grenoble cedex 9, France.

■ ACKNOWLEDGMENTS

The authors acknowledge David Bouville for sample preparation, Pascal Marie for fabrication of mechanical elements used in the measurement setup, Rafael Salas-Montiel and Aurelien Bruyant for participation to near-field setup development. They also thank Gilles Lerondel and Pierre Beauvillain for fruitful discussions. This work has been supported by the Agence Nationale de la Recherche under contract PLACIDO No. ANR-08-BLAN-0285-01. Mickaël Février grant has been funded by Région Ile-de-France.

■ REFERENCES

(1) Quinten, M.; Leitner, A.; Krenn, J. R.; Aussenegg, F. R. Electromagnetic energy transport via linear chains of silver nanoparticles. *Opt. Lett.* **1998**, *23*, 1331−1333.
(2) Brongersma, M. L.; Hartman, J. W.; Atwater, H. A. Electromagnetic energy transfer and switching in nanoparticle chain arrays below the diffraction limit. *Phys. Rev. B* **2000**, *62*, R16 356−R16 359.
(3) Krenn, J. R.; et al. Squeezing the optical near-field zone by plasmon coupling of metallic nanoparticles. *Phys. Rev. Lett.* **1999**, *82*, 2590−2593.
(4) Maier, S. A.; et al. Local detection of electromagnetic energy transport below the diffraction limit in metal nanoparticle plasmon waveguides. *Nat. Mater.* **2003**, *2*, 229−232.
(5) Femius Koenderink, A.; de Waele, R.; Prangsma, J. C.; Polman, A. Experimental evidence for large dynamic effects on the plasmon dispersion of subwavelength metal nanoparticle waveguides. *Phys. Rev. B* **2007**, *76*, 201403(R).
(6) Crozier, K. B.; Togan, E.; Simsek, E.; Yang, T. Experimental measurement of the dispersion relations of the surface plasmon modes of metal nanoparticle chains. *Opt. Express* **2007**, *15*, 17482−17493.
(7) De Waele, R.; Femius Koenderink, A.; Polman, A. Tunable nanoscale localization of energy on plasmon particle arrays. *Nano Lett.* **2007**, *7*, 2004−2008.
(8) Neutens, P.; Van Dorpe, P.; De Vlaminck, I.; Lagae, L.; Borghs, G. Electrical detection of confined gap plasmons in metal-insulator-metal waveguides. *Nat. Photonics* **2009**, *3*, 283−286.
(9) Bozhevolnyi, S. I.; Volkov, V. S.; Devaux, E.; Ebbesen, T. W. Channel plasmon-polariton guiding by subwavelength metal grooves. *Phys. Rev. Lett.* **2005**, *95*, 046802.
(10) Barnes, W. L.; Dereux, A.; Ebbesen, T. W. Surface plasmon subwavelength optics. *Nature* **2003**, *424*, 824−511.
(11) Bozhevolnyi, S. I.; Volkov, V. S.; Devaux, E.; Laluet, J.-Y.; Ebbesen, T. W. Channel plasmon subwavelength waveguide components including interferometers and ring resonators. *Nature* **2006**, *440*, 508−511.
(12) Zou, S.; Shatz, G. C. Metal nanoparticle array waveguides: proposed structures for subwavelength devices. *Phys. Rev. B* **2006**, *74*, 125111.
(13) Danckwerts, M.; Novotny, L. Optical frequency mixing at coupled gold nanoparticles. *Phys. Rev. Lett.* **2007**, *98*, 026104.
(14) Noginov, M. A.; et al. Demonstration of a spaser-based nanolaser. *Nature* **2009**, *460*, 1110−1113.
(15) Temnov, V. V.; et al. Active magneto-plasmonics in hybrid metal−ferromagnet structures. *Nat. Photonics.* **2010**, *4*, 107−111.
(16) Juan, M. L.; Righini, M.; Quidant, R. Plasmon nano-optical tweezers. *Nat. Photonics* **2011**, *5*, 349−356.
(17) Blaize, S.; et al. Real-space observation of spectral degeneracy breaking in a waveguide-coupled disk microresonator. *Opt. Lett.* **2010**, *35*, 3168−3170.
(18) Chuang, S. L. Physics of optoelectronic devices; John Wiley & Sons: New-York, 1995; Chapter 8.
(19) Marcatili, E. Improved coupled-mode equations for dielectric guides. *IEEE J. Quantum Electron.* **1986**, *QE-22*, 988−993.
(20) Delacour, C.; et al. Efficient directional coupling between silicon and copper plasmonic nanoslot waveguides: towards metal-oxide-silicon nanophotonics. *Nano Lett* **2010**, *10*, 2922−2926.
(21) Femius Koenderink, A.; Polman, A. Complex response and polariton-like dispersion splitting in periodic metal nanoparticle chains. *Phys. Rev. B* **2006**, *74*, 033402.
(22) Weber, W. H.; Ford, G. W. Propagation of optical excitations by dipolar interactions in metal nanoparticle chains. *Phys. Rev. B* **2004**, *70*, 125429.
(23) Simsek, E. On the surface resonance modes of metal nanoparticle chains and arrays. *Plasmonics* **2009**, *4*, 223−230.
(24) Torrado, J. F.; González-Díaz, J. B.; González, M. U.; García-Martín, A.; Armelles, G. Magneto-optical effects in interacting localized and propagating surface plasmon modes. *Opt. Express* **2010**, *18*, 15635−15642.
(25) Huang, C.; Bonroy, K.; Reekmans, G.; Laureyn, W.; Verhaegen, K.; de Vlaminck, I.; Lagae, L.; Borghs, G. Localized surface plasmon resonance biosensor integrated with microfluidic chip. *Biomed. Microdevices* **2009**, *11*, 893−901.